Supporting Information

Dendritic Sb_2Se_3/In_2S_3 Heterojunction Nanorod Arrays Photocathode Decorated with MoS_x Catalyst for Efficient Solar Hydrogen Evolution

*Chang Liu,[†a] Tao Liu,[†b] Yingzheng Li,[a] Ziqi Zhao,[a] Dinghua Zhou,[a] Wenlong Li,[a] Yilong Zhao,[a] Hao Yang,[c] Licheng Sun,[a,c,d] Fusheng Li,[*a] and Zhiqiang Li[*b]*

a) State Key Laboratory of Fine Chemicals, Institute of Artificial Photosynthesis, DUT-KTH Joint Education and Research Centre on Molecular Devices, Institute for Energy Science and Technology, Dalian University of Technology, 116024 Dalian, China. *fusheng@dlut.edu.cn*

b) National-Local Joint Engineering Laboratory of New Energy Photoelectric Devices, College of Physics Science and Technology, Hebei University, 071002 Baoding, China. *lizhiqiang@hbu.edu.cn*

c) Department of Chemistry, School of Engineering Sciences in Chemistry, Biotechnology and Health, KTH Royal Institute of Technology, Stockholm 10044, Sweden.

d) Center of Artificial Photosynthesis for Solar Fuels, School of Science, Westlake University, 310024 Hangzhou, China.

[†]These authors contributed equally to this work.

Instruments. The surface morphology of the fabricated films was characterized by field emission scan electron microscopy (FE-SEM, HITACHI SU8220, operate at 5 kV). The surface compositions and the band diagrams of the electrode films were investigated using X-ray photoelectron spectroscopy (XPS) and (ultraviolet photoelectron spectroscopy (UPS) on an ESCALAB Xi$^+$ (Thermo Scientific™), and the crystal structures were characterized by X-ray diffraction (XRD) with Cu Kα (1.54056 Å) radiation (SmartLab 9KW). The chemical structure of the films was studied using Raman spectroscopy at room temperature (LabRAM HR800, 532 nm excitation wavelength; HORIBA JobinYvon).

Materials. Molybdenum (Mo, 99.99%), antimony selenide (Sb_2Se_3, 99.99%) and selenium (Se powder, 99.99%) were purchased from Zhongnuo, Beijing, China. Thioacetamide (C_2H_5NS, 99%) and Citric acid ($C_6H_8O_7$, 99%) were purchased from Innochem Reagent, Beijing, China. Indium chloride ($InCl_3 \cdot 4H_2O$, 99.99%), Ammonium thiomolybdate ($(NH_4)_2MoS_4$, 99.95%) and Sodium perchlorate ($NaClO_4$, 98%) were purchased from Aladdin Reagent, Shanghai, China. All the reagents were used as received without further treatment. All aqueous solutions were prepared with high-purity deionized water (Milli-Q, resistance 18 MΩ cm^{-1}).

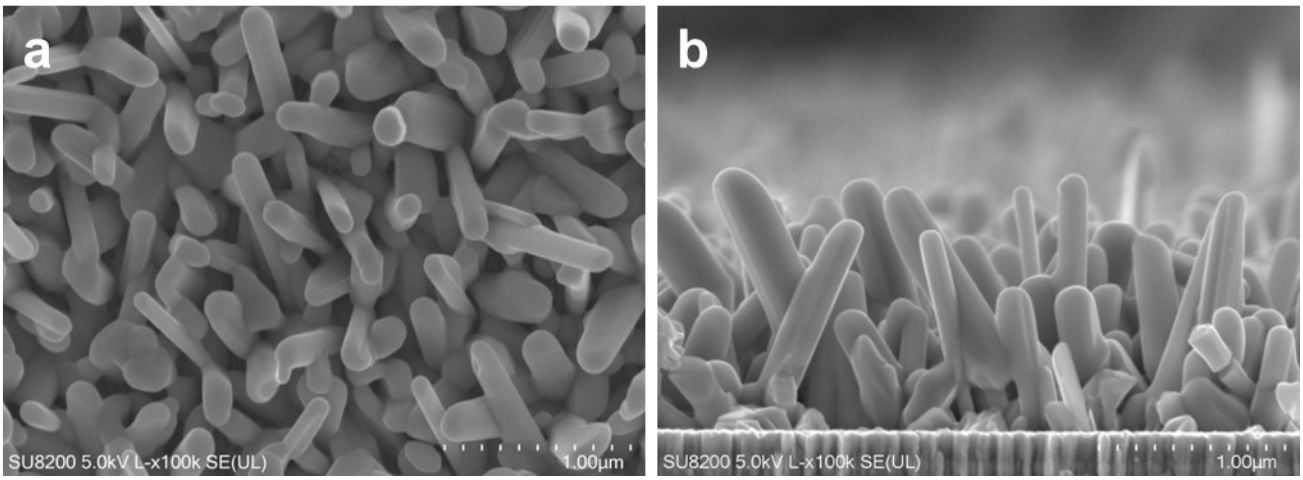

Figure S1. The top view (a) and cross view (b) SEM images of Sb_2Se_3 film.

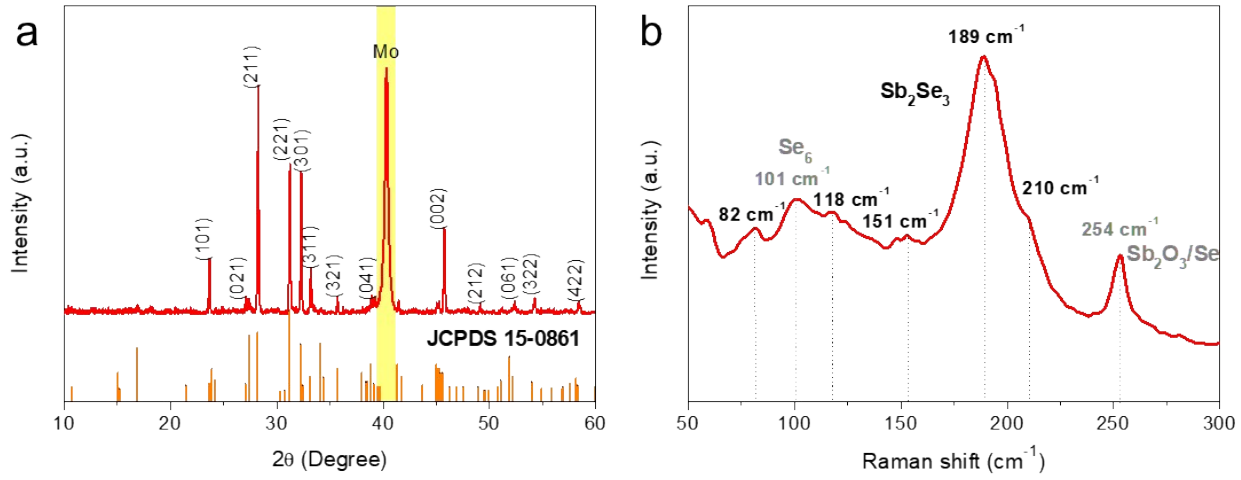

Figure S2. The XRD pattern (a) and Raman spectrum (b) of Sb_2Se_3 film.

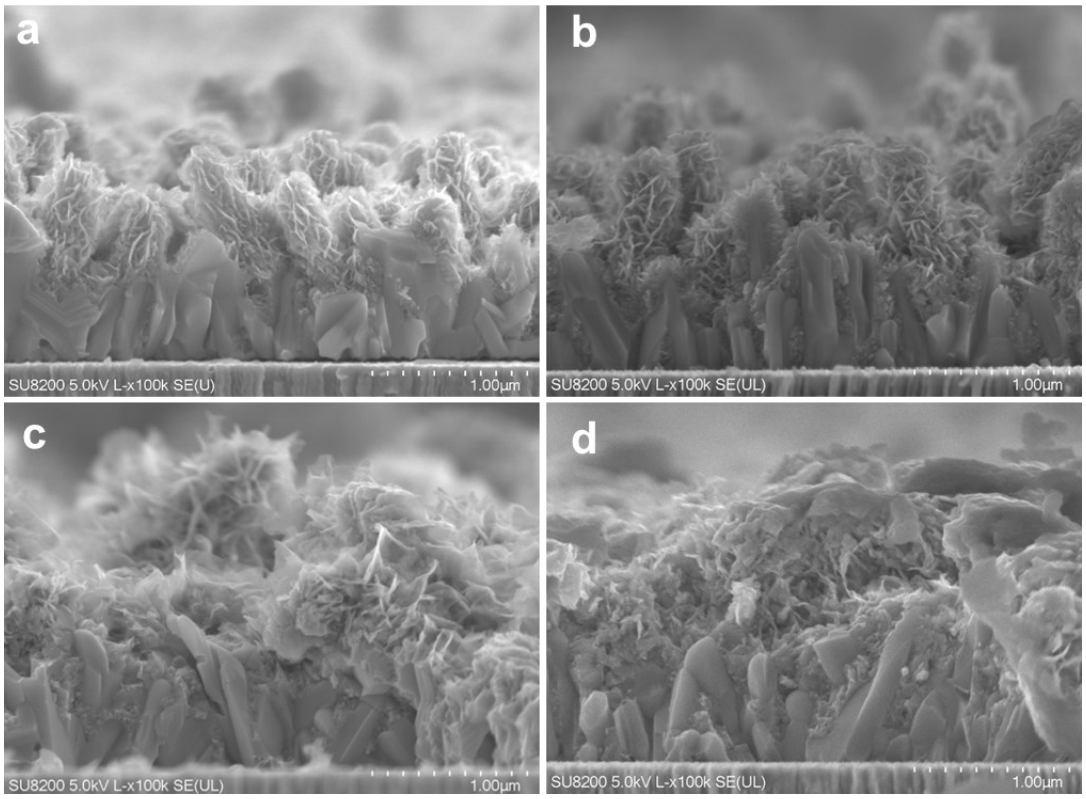

Figure S3. The cross-view SEM images of varying thickness In_2S_3 film grown on Sb_2Se_3, (a) Sb_2Se_3/In_2S_3-1.5, (b) Sb_2Se_3/In_2S_3-2, (c) Sb_2Se_3/In_2S_3-3, (d) Sb_2Se_3/In_2S_3-4.

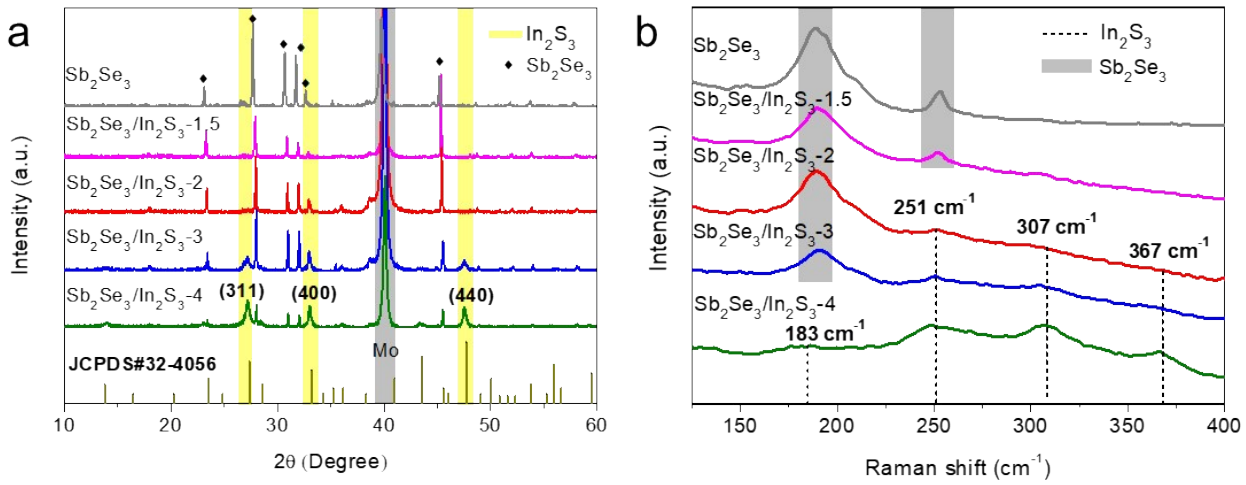

Figure S4. The XRD pattern (a) and Raman spectra (b) of Sb_2Se_3, Sb_2Se_3/In_2S_3-1.5, Sb_2Se_3/In_2S_3-2, Sb_2Se_3/In_2S_3-3 and Sb_2Se_3/In_2S_3-4 films.

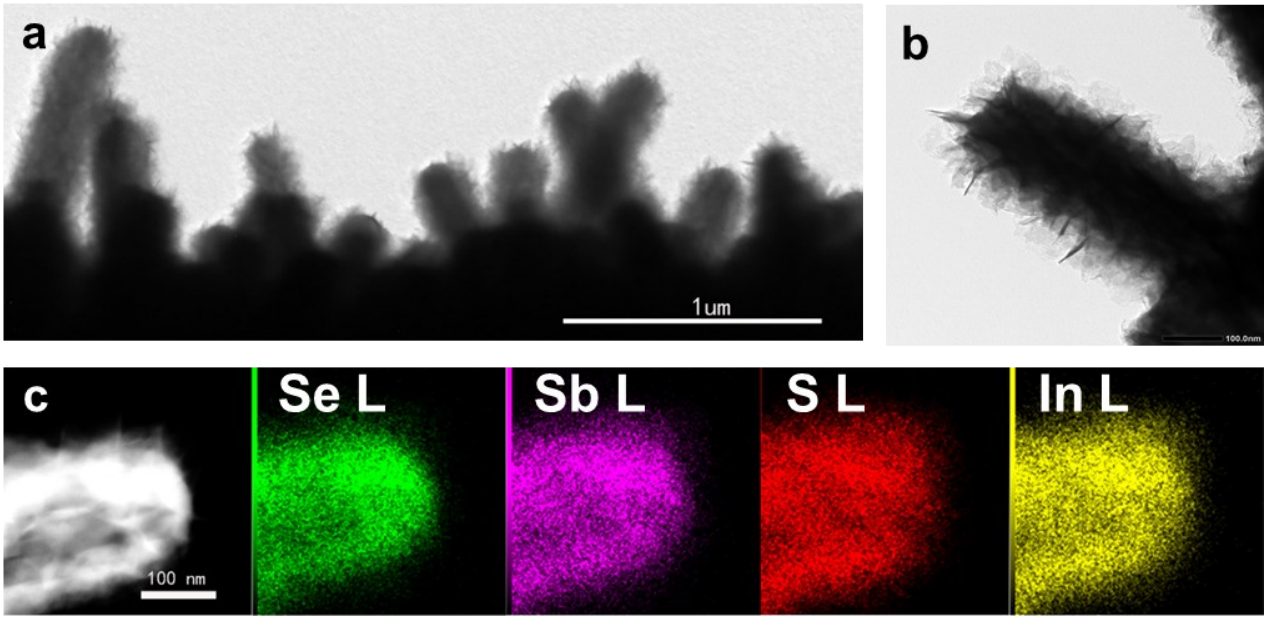

Figure S5. (a) and (b) the high-resolution transmission electron microscopy (HRTEM) images of Sb_2Se_3/In_2S_3-2 film, (c) the HAADF-STEM image and energy-dispersive spectroscopy elemental mapping of the Sb_2Se_3/In_2S_3-2 film. Elements detected: Se, Sb, S, and In, respectively.

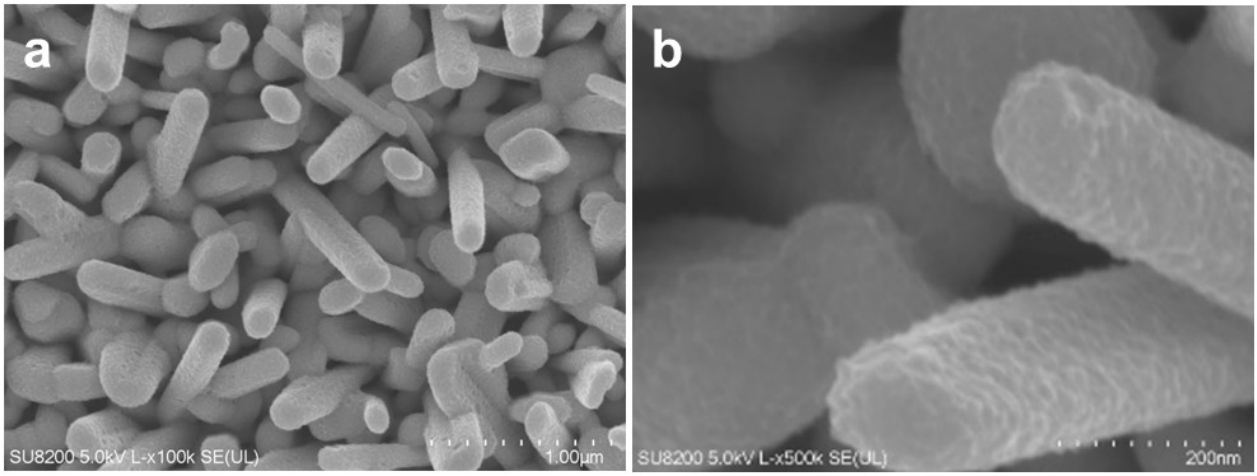

Figure S6. The surface SEM images of Sb_2Se_3/MoS_x.

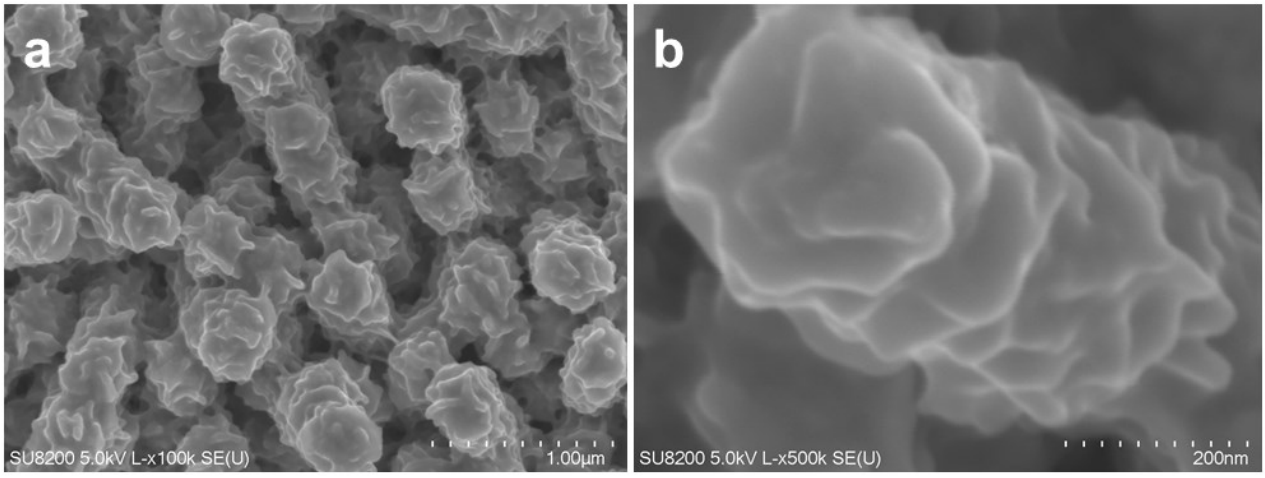

Figure S7. The surface SEM images of Sb_2Se_3/In_2S_3-2/MoS_x.

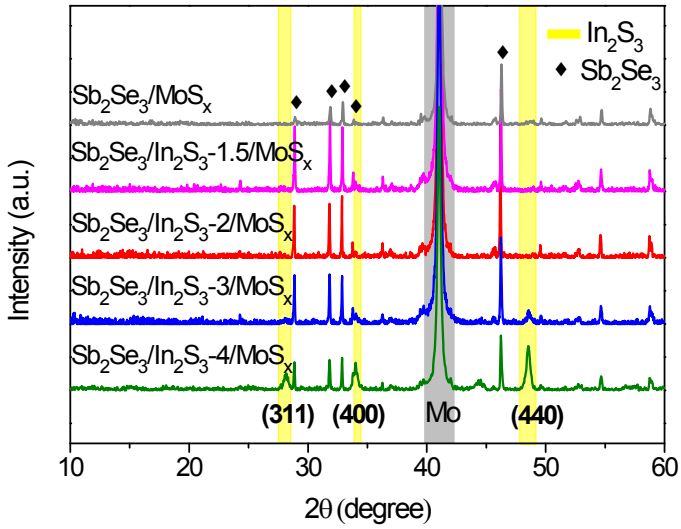

Figure S8. The XRD pattern of different $Sb_2Se_3/In_2S_3/MoS_x$ and Sb_2Se_3/MoS_x films.

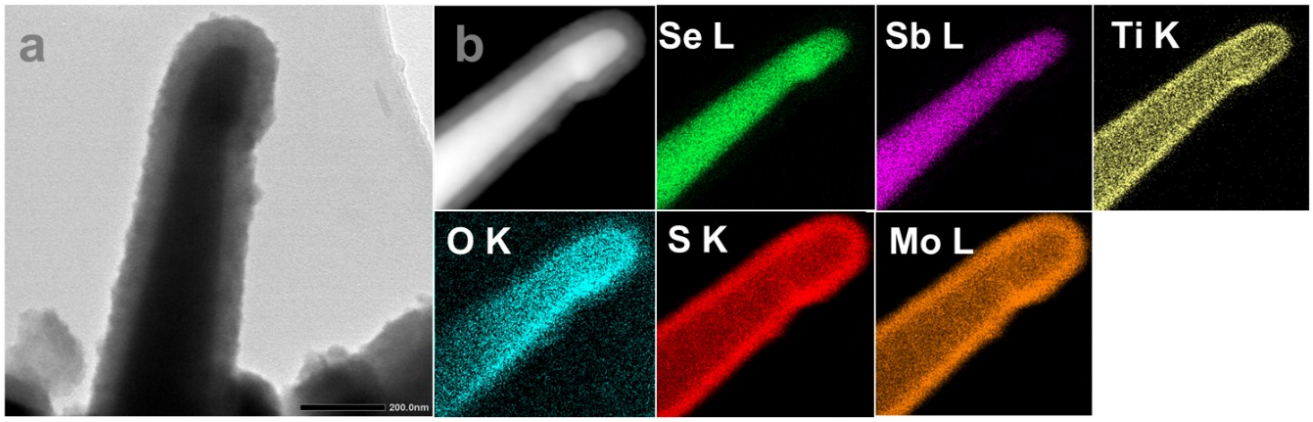

Figure S9. (a) the HRTEM image and (b) the HAADF-STEM and the corresponding EDS mapping images of the Sb_2Se_3/MoS_x films.

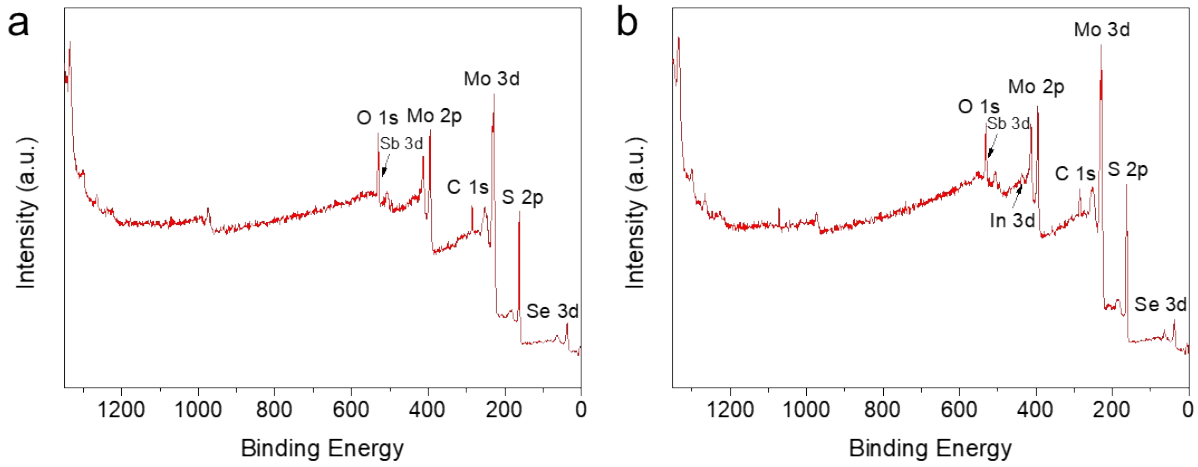

Figure S10. XPS survey spectra of (a) Sb_2Se_3/MoS_x film, (b) $Sb_2Se_3/In_2S_3/MoS_x$ film.

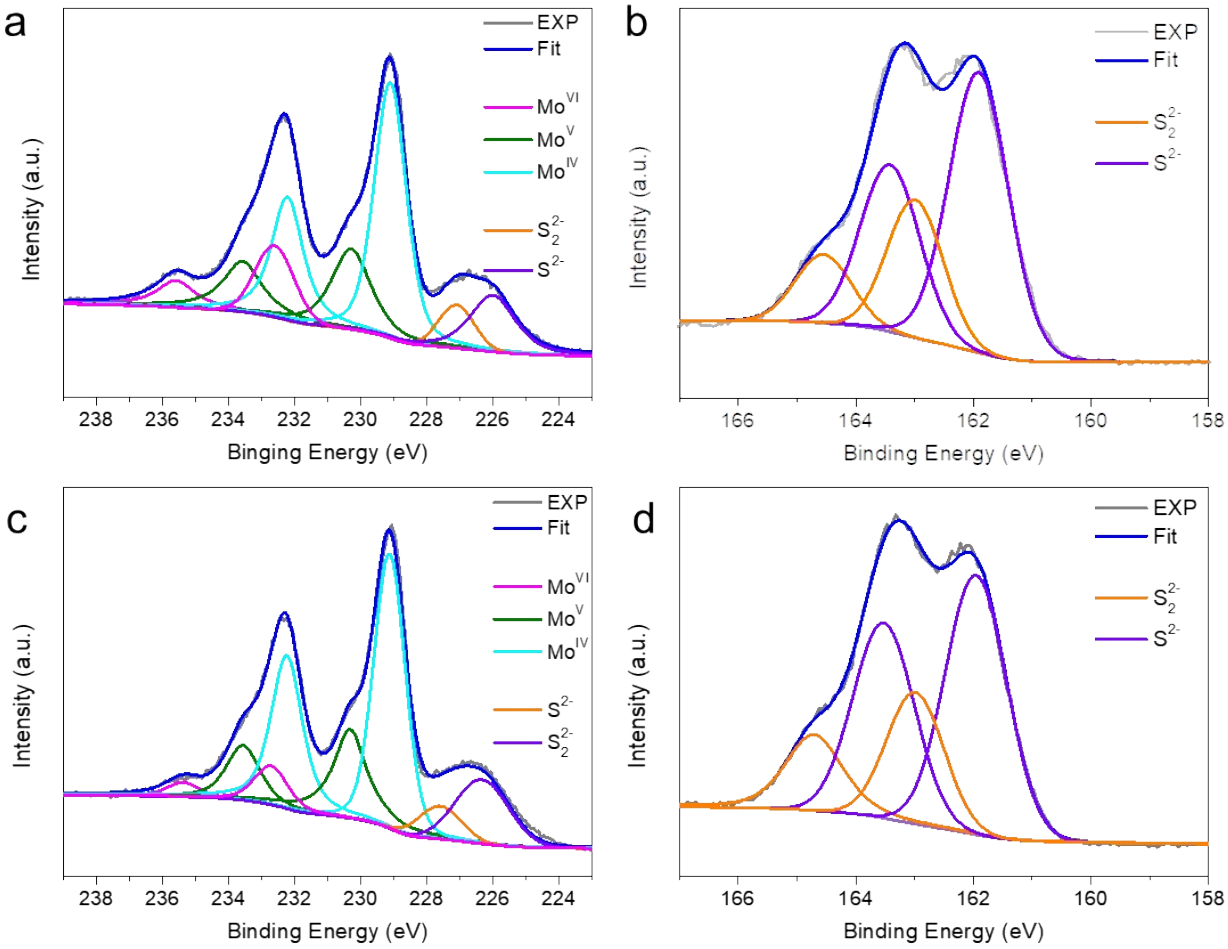

Figure S11. High-resolution XPS spectra of (a), (b) Sb_2Se_3/MoS_x, (c), (d) $Sb_2Se_3/In_2S_3/MoS_x$.

X-ray photoelectron spectra (XPS) fitting for the MoS_x catalysts on the surface of Sb_2Se_3 and Sb_2Se_3/In_2S_3 photocathode. (a), (c) In the Mo 3d and S 2s regions, the three doublets of Mo 3d are Mo^{VI}, Mo^{V}, and Mo^{IV} states, represented by purple-, pink-, and orange-colored peaks, respectively. The two peaks of S 2s are S_2^{2-}, and S^{2-}states, represented by blue- and green-colored peaks, respectively. (b), (d) In the S 2p regions, the two doublets of S 2p are S_2^{2-}, and S^{2-} states and the doublet of sulfate, represented by blue, green- and dark red-colored peaks, respectively.

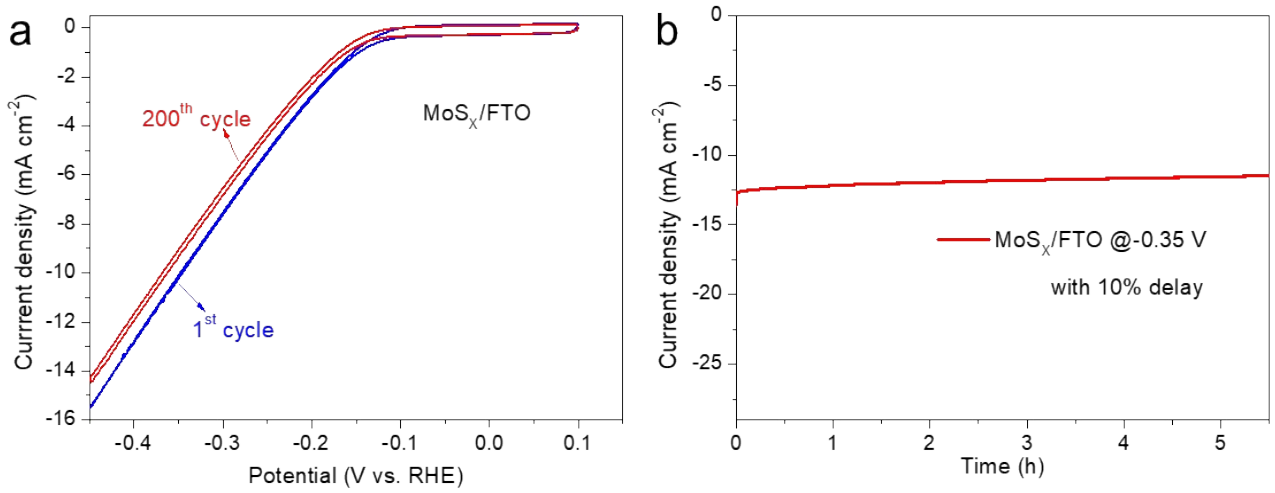

Figure S12. (a) The CV curves for MoS_X/FTO in 0.1 M H_2SO_4. The sweep rate was10 mV s^{-1}. (b) I-t curve of MoS_X/FTO at -0.35 V vs. RHE.

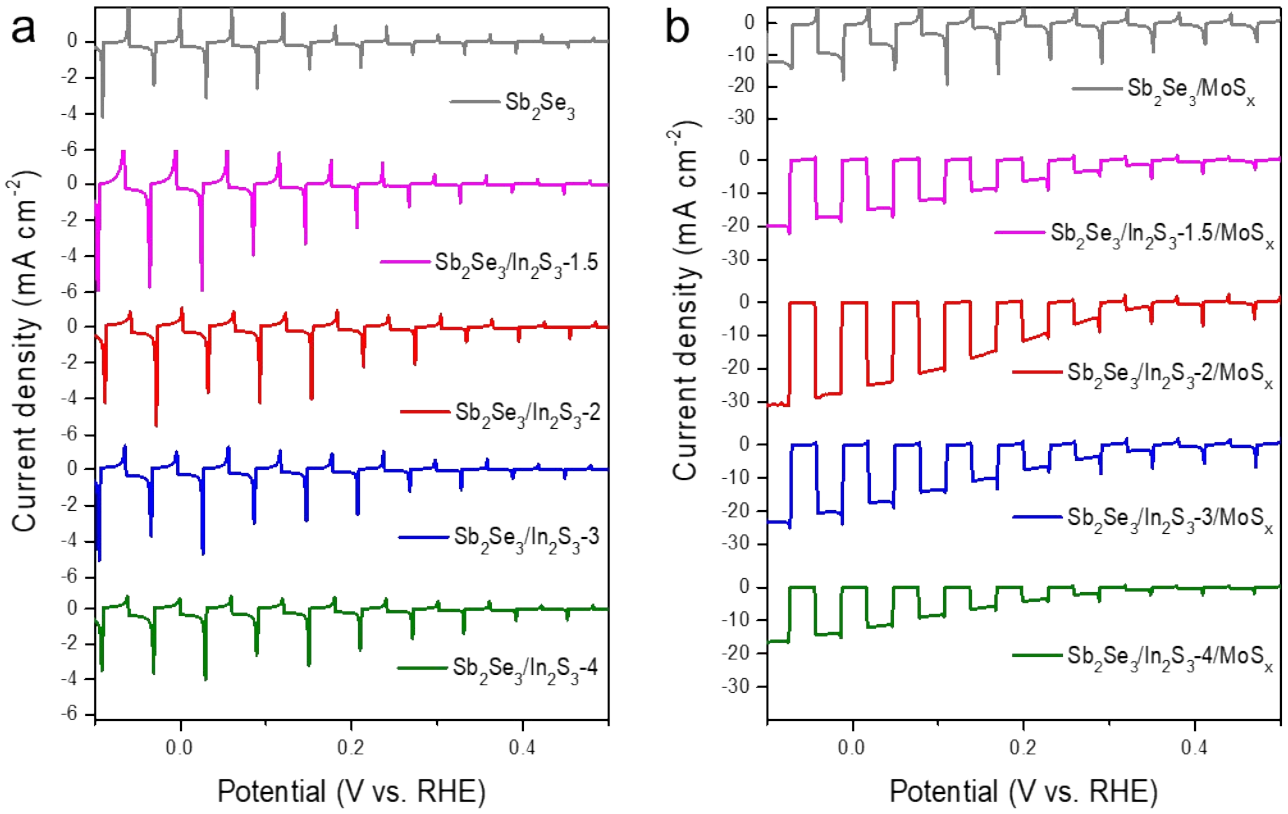

Figure S13. Current density−potential curves of (a) Sb_2Se_3 and Sb_2Se_3/In_2S_3 photocathodes, (b) Sb_2Se_3/MoS_x and $Sb_2Se_3/In_2S_3/MoS_x$ photocathodes in a 0.1 M H_2SO_4 electrolyte under chopped illumination (AM 1.5 G,100 mW cm^{-2}).

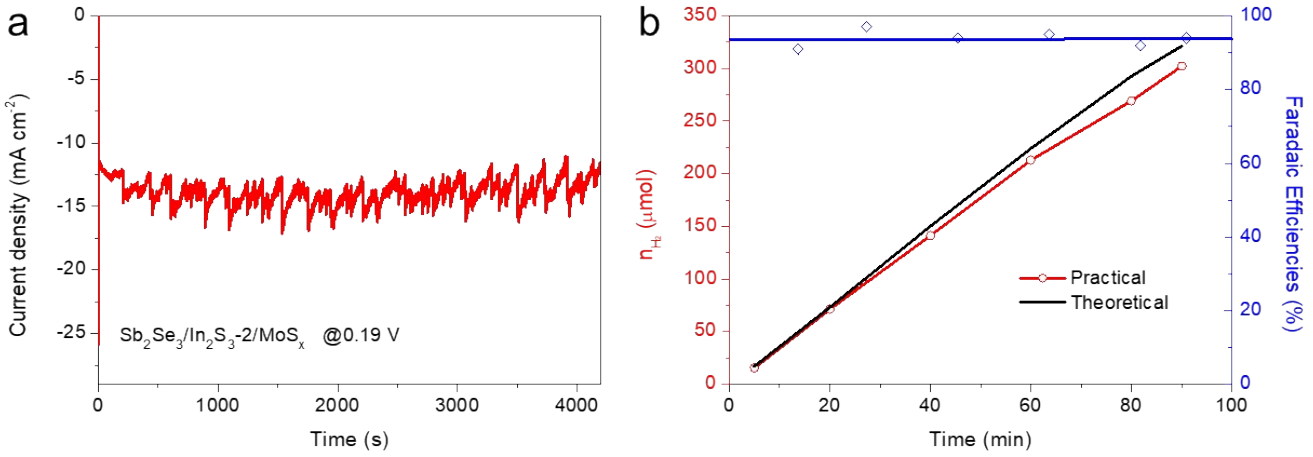

Figure S14. (a) *I-t* curve of Sb_2Se_3/In_2S_3-2/MoS_x photocathode at 0.19 V vs RHE under illumination (AM 1.5 G,100 mW cm^{-2}). (b) The Faradaic efficiency of Sb_2Se_3/In_2S_3-2/MoS_x photocathode for HER. Hydrogen evolution detected by gas chromatography and the charge passed during the photolysis of Sb_2Se_3/In_2S_3-2/MoS_x photocathode at an applied potential of 0.19 V vs RHE.

To measure the amount of hydrogen produced by the photoelectrochemical process, chronopotentiometry measurements were recorded in a sealed quartz cell (0.1 M H_2SO_4, as electrolyte, Sb_2Se_3/In_2S_3-2/MoS_x as work electrode) at an applied potential of 0.19 V vs. RHE without iR compensation. Before chronopotentiometry measurement, the assembled quartz cell was degassed by argon for 40 min. 0.5 mL of gas was analyzed by gas chromatography (GC, Techcomp GC 7890T, Ar carrier gas, Thermo Conductivity Detector). The theoretical H_2 evolution can be calculated by the amount of charge passed through electrodes. The red square is the experimental data and the black line is the theoretical value of hydrogen, the blue square is the corresponding Faradaic efficiency and the blue line is the average Faradaic Efficiency.

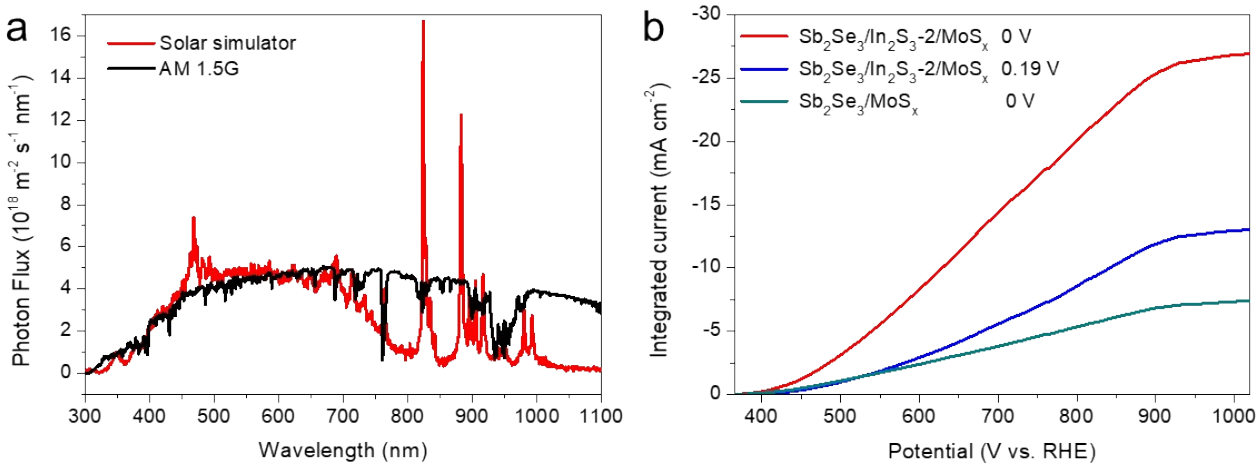

Figure S15. Properties of the solar simulator. (a) Solar irradiance of the AM 1.5G (ASTM G173-03) and the solar simulator. (b) The calculated photocurrents of Sb_2Se_3/MoS_x at 0 V vs RHE, $Sb_2Se_3/In_2S_3/MoS_x$ at 0.19 V vs RHE and 0 V vs RHE by integrating IPCE over the photon flux of AM 1.5G (ASTM G173-03).

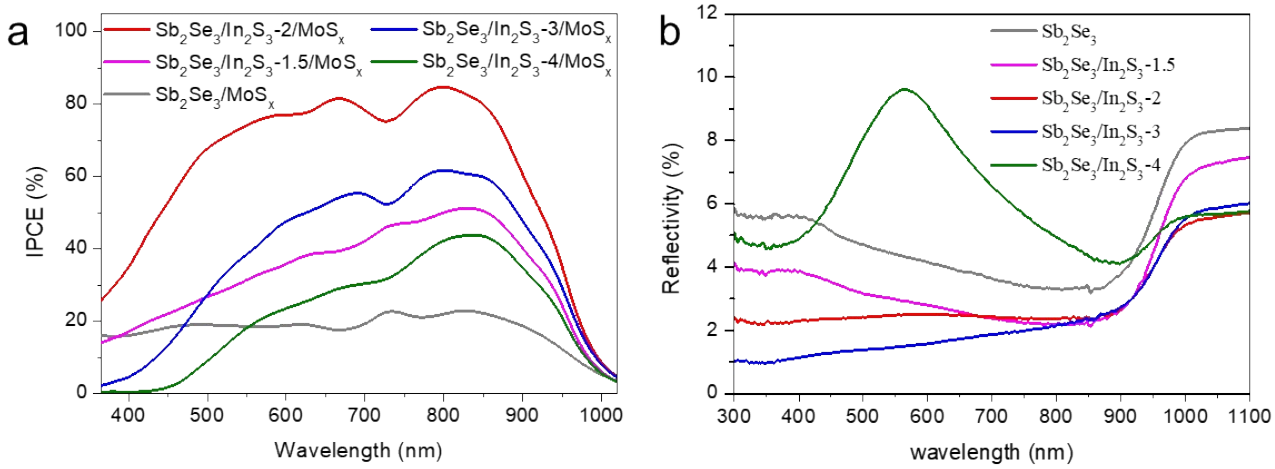

Figure S16. (a) Incident photon-to-current efficiencies (IPCE) of Sb_2Se_3/MoS_x and $Sb_2Se_3/In_2S_3/MoS_x$ photocathodes at 0 V vs RHE. (b) Reflectance spectra of Sb_2Se_3 and four different Sb_2Se_3/In_2S_3 films measured by solid UV-Vis spectrometer.

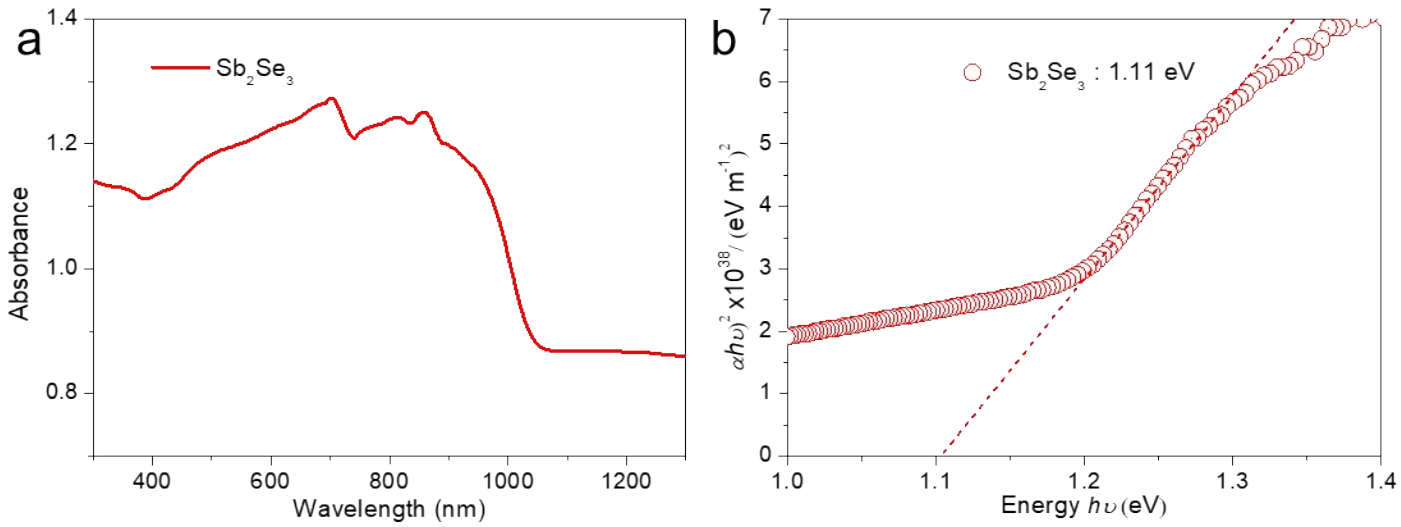

Figure S17. (a) Absorbance spectrum and (b) Tauc plot of Sb_2Se_3 reference thin film. The bandgap of Sb_2Se_3 is determined to be 1.11 eV.

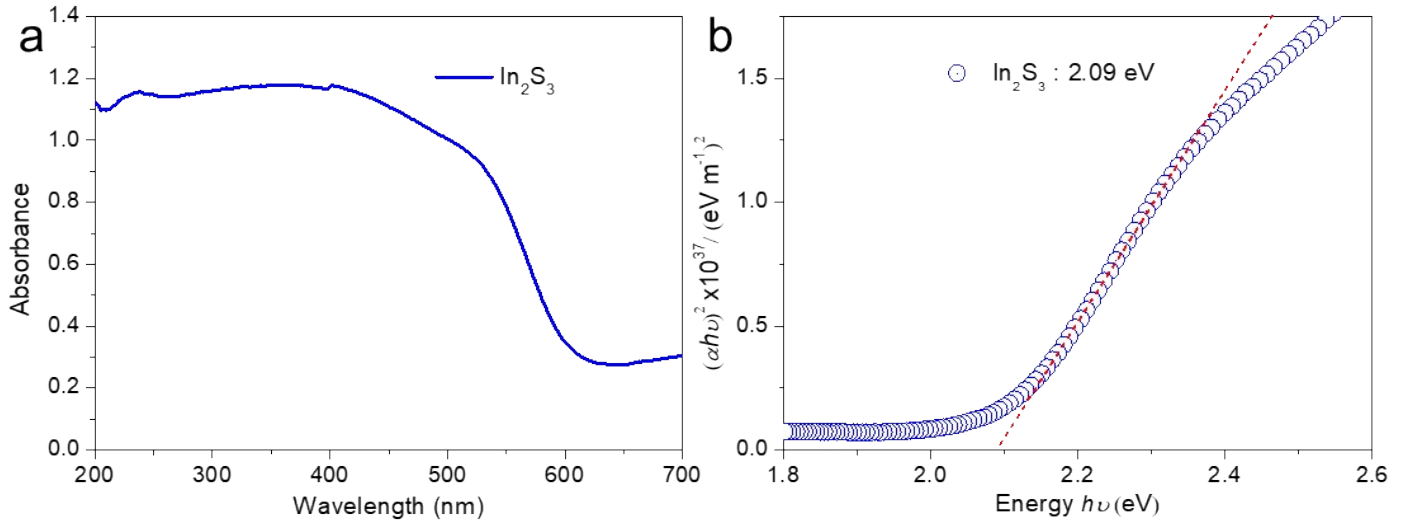

Figure S18. (a) Absorbance spectrum and (b) Tauc plot of In_2S_3 reference thin film (deposited on FTO). The bandgap of In_2S_3 is determined to be 2.09 eV.

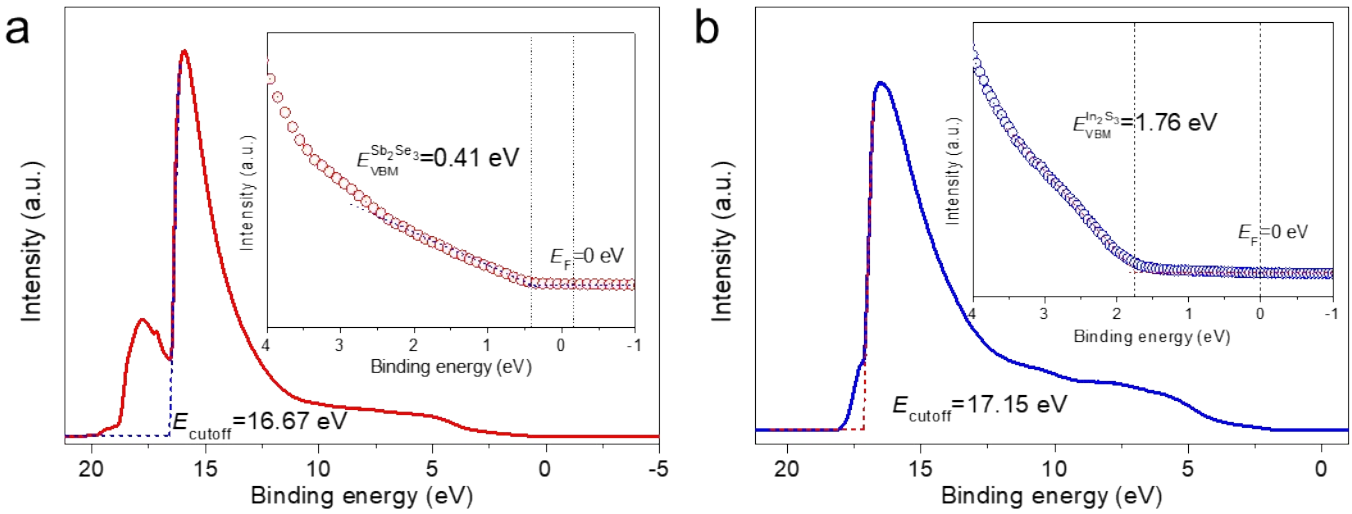

Figure S19. UPS spectra of the Sb_2Se_3, Sb_2Se_3/In_2S_3 for VB determination. The insert show the enlarged valence band position of Sb_2Se_3 and In_2S_3, respectively.

The work function (E_{work} corresponding to the Fermi level), valence band (VB), and conduction band (CB) of Sb_2Se_3 and Sb_2Se_3/In_2S_3 were determined according to following equations.

$$E_{\text{work}} = \text{h}\nu - \left(E_{\text{cutoff}} - E_F\right) \qquad equation\ S1$$

$$E_{VB} = E_{\text{work}} + E_{VBM} \qquad equation\ S2$$

$$E_{CB} = E_{VB} - E_{\text{g}} \qquad equation\ S3$$

Where, the E_{cutoff} is cut-off energy edge, the E_F is initial edge energy, the E_{VBM} is the energy from valence band maximum to Fermi level, the E_g is band gap energy (obtained by UV-vis spectra), the E_{VB} is valance band energy and the E_{CB} is conduction band energy.

For Sb_2Se_3 electrode,

$E_{\text{work}} = 21.2 - \left(16.67 - 0\right) = 4.53$ eV; $E_{VB} = 4.53 + 0.41 = 4.94$ eV; and $E_{CB} = 4.94 - 1.11 = 3.83$ eV.

For the Sb_2Se_3/In_2S_3 heterojunction,

$E_{\text{work}} = 21.2 - \left(17.15 - 0\right) = 4.05$ eV; $E_{VB} = 4.05 + 1.76 = 5.81$ eV; and $E_{CB} = 5.81 - 2.09 = 3.72$ eV.

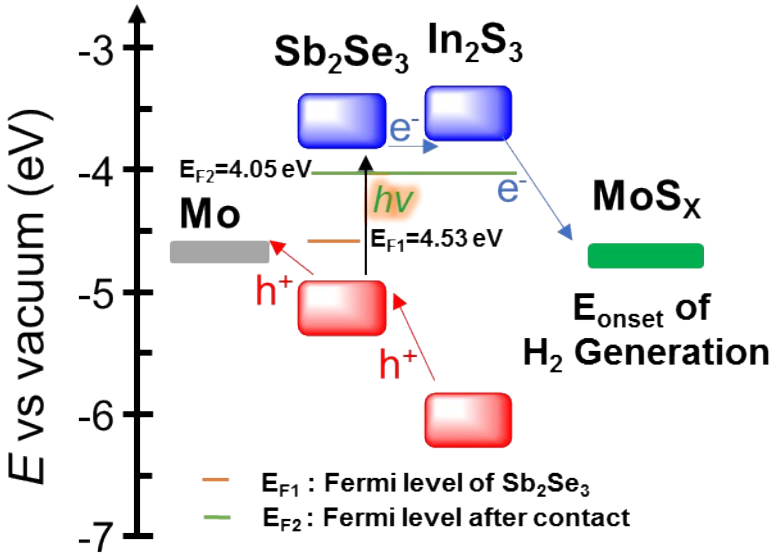

Figure. S20 The band alignment diagram of the $Sb_2Se_3/In_2S_3/MoS_X$ photocathode.

Table S1. Summary of PEC performance of recent published photocathodes.

Device structure	Current density at 0 V vs RHE (mA cm^{-2})	Electrolyte	Onset Potential (V vs. RHE)	ABPE (%)	Stability (J/J_0); Time	Ref.
$Mo/Sb_2Se_3/In_2S_3/TiO_2/MoS_x$	**27**	**0.1 M H_2SO_4**	**0.39**	**2.6**	**100%; 1.5 h**	**This work**
$FTO/Au/Sb_2Se_3/CdS/TiO_2/Pt$	20	pH 1 H_2SO_4	0.5	3.40	--	1
$FTO/Au/Sb_2Se_3/TiO_2/RuO_x$	30	pH 1 H_2SO_4	0.41	2.33	--	1
FTO/Au/bilayer $Sb_2Se_3/TiO_2/C_{60}/Pt$	30	pH 1 H_2SO_4	0.32	--	~100%; 10 h	2
$Mo/Sb_2Se_3/TiO_2/Pt$	20.2	1 M H_2SO_4	0.57	1.36	85%; 10 h	3
$FTO/Cu:NiO_x/Sb_2Se_3/TiO_2/Pt$	17.5	pH 1 H_2SO_4	0.34	--	75%; 4 h	4
$FTO/Au/Sb_2Se_3/TiO_2/C_{60}/Pt$	17	pH 1 H_2SO_4	0.55	--	98%; 10 h	5
$FTO/Au/Sb_2Se_3/TiO_2/MoS_x$	14	1 M H_2SO_4	0.2	--	70%; 2 h	6
$FTO/Au/Sb_2Se_3/CdS/TiO_2/Pt$	13.5	pH 1 H_2SO_4	0.47	--	73%; 3 h	7
$n+p\text{-}Si/Al_2O_3/MoS_2$	34.5	pH 0.3 H_2SO_4	0.35	~2	~100%; 40 h	8
$n+p\text{-}Si/MoS_2$	17.5	1 M H_2SO_4	0.4	~2	~100%; 100 h	9
$n+p\text{-}Si/Ti\text{-}TiO_x/MoS_x$	16	1 M $HClO_4$	0.33	--	75%; 10 h	10
$FTO/Au/Cu_2O/TiO_2/MoS_{2+x}$	6.3	1 M KOH	~0.5	--	~100%;10 h	11
$FTO/Au/Cu_2O/AZO/TiO_2/MoS_x$	5.7	pH 1 H_2SO_4	0.46	--	~17%; 7 h	12
$GaAs/GaInP_2/TiO_2/g\text{-}MoS_x$	8.5	1 M H_2SO_4	0.2	--	80%; 20 h	13
$Au/InP/Ti/MoS_x$	15.8	1 M $HClO_4$	0.62	--	~100%; 2 h	14

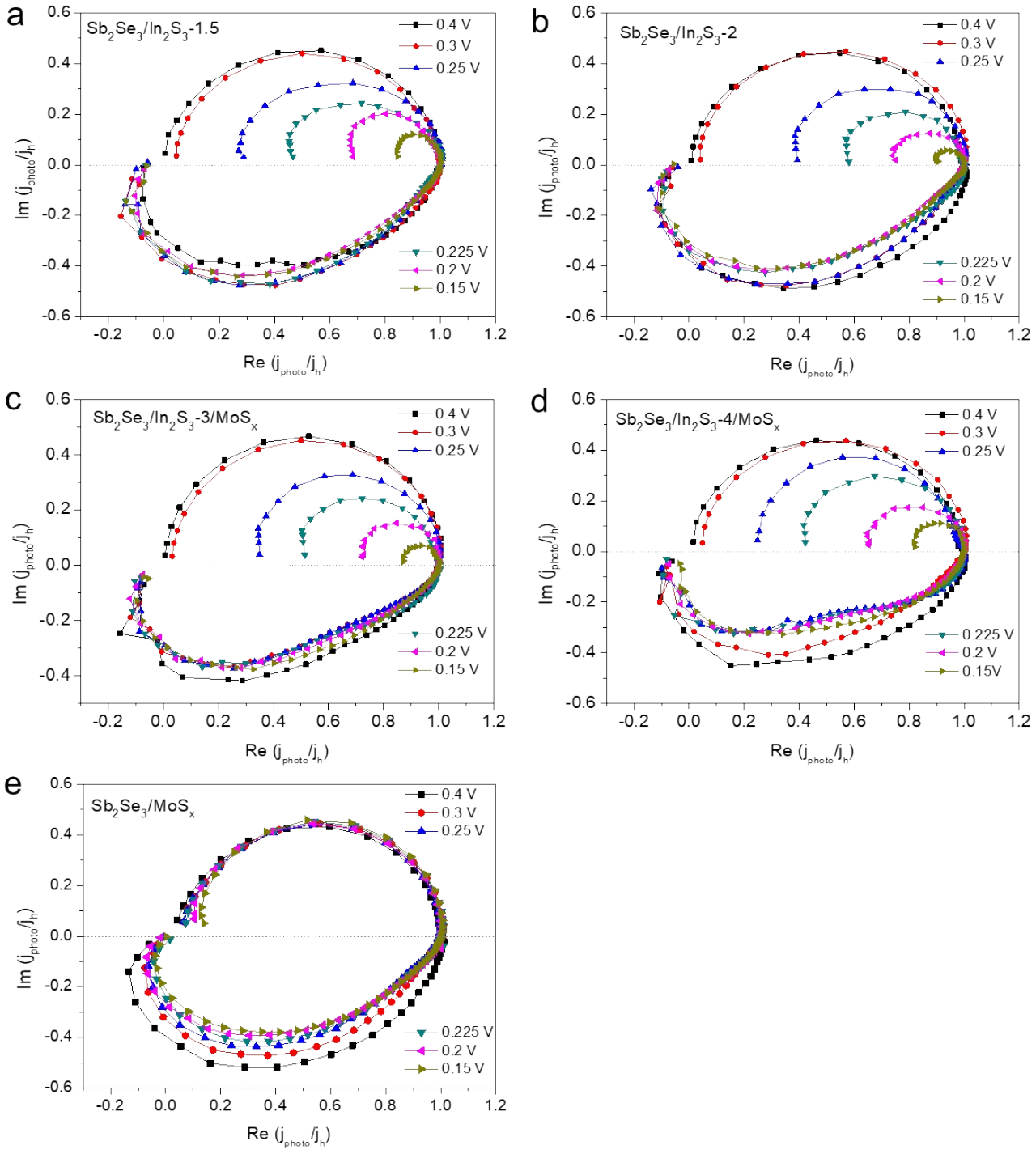

Figure S21. IMPS spectra of Sb_2Se_3/MoS_x and $Sb_2Se_3/In_2S_3/MoS_x$ photocathodes at various potential.

Table S2. The values of resistances and capacitances in fitted EC.

Device Structure	R_s (Ω)	R_{bulk} (Ω)	C_{bulk} (F)	R_{ct} (Ω)	C_H (F)
Sb_2Se_3/MoS_x	14.4	31.6	1.19μ	22.4	1.34m
Sb_2Se_3/In_2S_3-1.5/MoS_x	15.6	29.2	3.24μ	7.66	2.37m
Sb_2Se_3/In_2S_3-2/MoS_x	11.8	17.4	4.48μ	6.42	5.73m
Sb_2Se_3/In_2S_3-3/MoS_x	10.57	21.3	3.61μ	6.95	5.11m
Sb_2Se_3/In_2S_3-4/MoS_x	12.0	45.7	1.05μ	9.20	1.61m

References

(1) Yang, W.; Kim, J. H.; Hutter, O. S.; Phillips, L. J.; Tan, J.; Park, J.; Lee, H.; Major, J. D.; Lee, J. S.; Moon, J. Benchmark Performance of Low-Cost Sb_2Se_3 Photocathodes for Unassisted Solar Overall Water Splitting. *Nat. Commun.* **2020,** *11*, 861.

(2) Park, J.; Yang, W.; Tan, J.; Lee, H.; Yun, J. W.; Shim, S. G.; Park, Y. S.; Moon, J. Hierarchal Nanorod-Derived Bilayer Strategy to Enhance the Photocurrent Density of Sb_2Se_3 Photocathodes for Photoelectrochemical Water Splitting. *ACS Energy Lett.* **2020,** *5*, 136-145.

(3) Zhou, H.; Feng, M.; Song, K.; Liao, B.; Wang, Y.; Liu, R.; Gong, X.; Zhang, D.; Cao, L.; Chen, S. A Highly [001]-Textured Sb_2Se_3 Photocathode for Efficient Photoelectrochemical Water Reduction. *Nanoscale* **2019,** *11*, 22871-22879.

(4) Lee, H.; Yang, W.; Tan, J.; Oh, Y.; Park, J.; Moon, J. Cu-Doped Niox as an Effective Hole-Selective Layer for a High-Performance Sb_2Se_3 Photocathode for Photoelectrochemical Water Splitting. *ACS Energy Lett.* **2019,** *4*, 995-1003.

(5) Tan, J.; Yang, W.; Oh, Y.; Lee, H.; Park, J.; Boppella, R.; Kim, J.; Moon, J. Fullerene as a Photoelectron Transfer Promoter Enabling Stable TiO_2-Protected Sb_2Se_3 Photocathodes for Photo-Electrochemical Water Splitting. *Adv. Energy Mater.* **2019,** *9*, 1900179.

(6) Prabhakar, R. R.; Septina, W.; Siol, S.; Moehl, T.; Wick-Joliat, R.; Tilley, S. D. Photocorrosion-Resistant Sb_2Se_3 Photocathodes with Earth Abundant Mosx Hydrogen Evolution Catalyst. *J. Mater. Chem. A* **2017,** *5*, 23139-23145.

(7) Park, J.; Yang, W.; Oh, Y.; Tan, J.; Lee, H.; Boppella, R.; Moon, J. Efficient Solar-to-Hydrogen Conversion from Neutral Electrolytes Using Morphology-Controlled Sb_2Se_3 Light Absorbers. *ACS Energy Lett.* **2019,** *4*, 517-526.

(8) Zhou, J.; Dai, S.; Dong, W.; Su, X.; Fang, L.; Zheng, F.; Wang, X.; Shen, M. Efficient and Stable MoS_2 Catalyst Integrated on Si Photocathodes by Photoreduction and Post-Annealing for Water Splitting. *Appl. Phys. Lett.* **2016,** *108*, 213905.

(9) Benck, J. D.; Lee, S. C.; Fong, K. D.; Kibsgaard, J.; Sinclair, R.; Jaramillo, T. F. Designing Active and Stable

Silicon Photocathodes for Solar Hydrogen Production Using Molybdenum Sulfide Nanomaterials. *Adv. Energy Mater.* **2014,** *4*, 1400739.
(10) Seger, B.; Laursen, A. B.; Vesborg, P. C. K.; Pedersen, T.; Hansen, O.; Dahl, S.; Chorkendorff, I. Hydrogen Production Using a Molybdenum Sulfide Catalyst on a Titanium-Protected n^+p-Silicon Photocathode. *Angew. Chem. Int. Ed.* **2012,** *51*, 9128-9131.
(11) Morales-Guio, C. G.; Liardet, L.; Mayer, M. T.; Tilley, S. D.; Grätzel, M.; Hu, X. Photoelectrochemical Hydrogen Production in Alkaline Solutions Using Cu_2O Coated with Earth-Abundant Hydrogen Evolution Catalysts. *Angew. Chem. Int. Ed.* **2015,** *54*, 664-667.
(12) Morales-Guio, C. G.; Tilley, S. D.; Vrubel, H.; Grätzel, M.; Hu, X. Hydrogen Evolution from a Copper(I) Oxide Photocathode Coated with an Amorphous Molybdenum Sulphide Catalyst. *Nat. Commun.* **2014,** *5*, 3059.
(13) Gu, J.; Aguiar, J. A.; Ferrere, S.; Steirer, K. X.; Yan, Y.; Xiao, C.; Young, James L.; Al-Jassim, M.; Neale, N. R.; Turner, J. A. A Graded Catalytic–Protective Layer for an Efficient and Stable Water-Splitting Photocathode. *Nat. Energy* **2017,** *2*, 16192.
(14) Li, Q.; Zheng, M.; Zhong, M.; Ma, L.; Wang, F.; Ma, L.; Shen, W. Engineering MoS_x/Ti/InP Hybrid Photocathode for Improved Solar Hydrogen Production. *Sci. Rep.* **2016,** *6*, 29738.